ELSEVIER

Earth and Planetary Science Letters 171 (1999) 661–671

EPSL

www.elsevier.com/locate/epsl

The flooding of Sundaland during the last deglaciation: imprints in hemipelagic sediments from the southern South China Sea

Carles Pelejero [a], Markus Kienast [b,c], Luejiang Wang [b,d], Joan O. Grimalt [a,*]

[a] *Department of Environmental Chemistry (ICER–CSIC), E-08034 Barcelona, Catalonia, Spain*
[b] *Geologisch–Paläontologisches Institut, University of Kiel, D-24098 Kiel, Germany*
[c] *Earth and Ocean Sciences, University of British Columbia, Vancouver, B.C., V6T 1Z4, Canada*
[d] *Department of Geoscience, Graduate School of Environmental Earth Science, Hokkaido University, Sapporo, 060-0810, Japan*

Received 4 March 1999; revised version received 2 July 1999; accepted 15 July 1999

Abstract

During the last 30 ka, the South China Sea (SCS) experienced pronounced palaeogeographic changes associated with the postglacial sea level rise, which significantly modified the hydrography of this marginal sea. The most crucial effects in the southern part of the basin were the submergence of Sundaland and the opening of the southern channels connecting the SCS to the tropical Indo-Pacific. Isotopic, sedimentological and organic geochemical parameters determined in two sediment cores from the southern SCS, one in the open sea and the other close to the continental shelf (sites 17961 and 17964, respectively) show that the main hydrographical changes during this period were related to critical thresholds in sea level rise. The main changes occurred at about 15–13.5 ky BP, coincident with Meltwater Pulse (MWP) Ia, when sea surface temperatures (SSTs) at both sites experienced a rapid 1.5ºC rise, and the clay content and *n*-nonacosane concentrations dropped significantly. Both trends reflect a rapid retreat of the coastline and an initial flooding of Sundaland at that time. A second important change, starting with the beginning of MWP Ib at about 11.5 ky BP and culminating at 10 ky BP, involved the establishment of modern hydrographic conditions. This is evident from the rapid convergence of the foraminiferal oxygen isotope records and the establishment of Holocene SST values. These results highlight the need to include the flooding/emergence of Sundaland as an important boundary condition in future modelling studies of Asian palaeomonsoons.

Keywords: South China Sea; biomarkers; eustacy; sea-level changes

1. Introduction

Eustatic sea level changes during the last glacial–interglacial cycle significantly altered the land-sea configuration and coastline location in the marginal basins of the western Pacific, where the largest shelf areas in the world, with water depths of 70–80 m, are located [1–3]. In the southern South China Sea (SCS), a vast area, Sundaland, emerged during the glacial sea level low stand [4] (Fig. 1) and a drainage system, the Molengraaff River, developed in this emergent tropical lowland [5,6] (Fig. 1). Recent modelling studies (e.g. [7,8]) suggest a critical linkage between hydrological phenomena in the Western Pacific Warm Pool (WPWP) and global climate vari-

* Corresponding author. Tel.: +34 93 4006122; Fax: +34 93 2045904; E-mail: jgoqam@cid.csic.es

0012-821X/99/$ – see front matter
PII: S0012-821X(99)00178-8

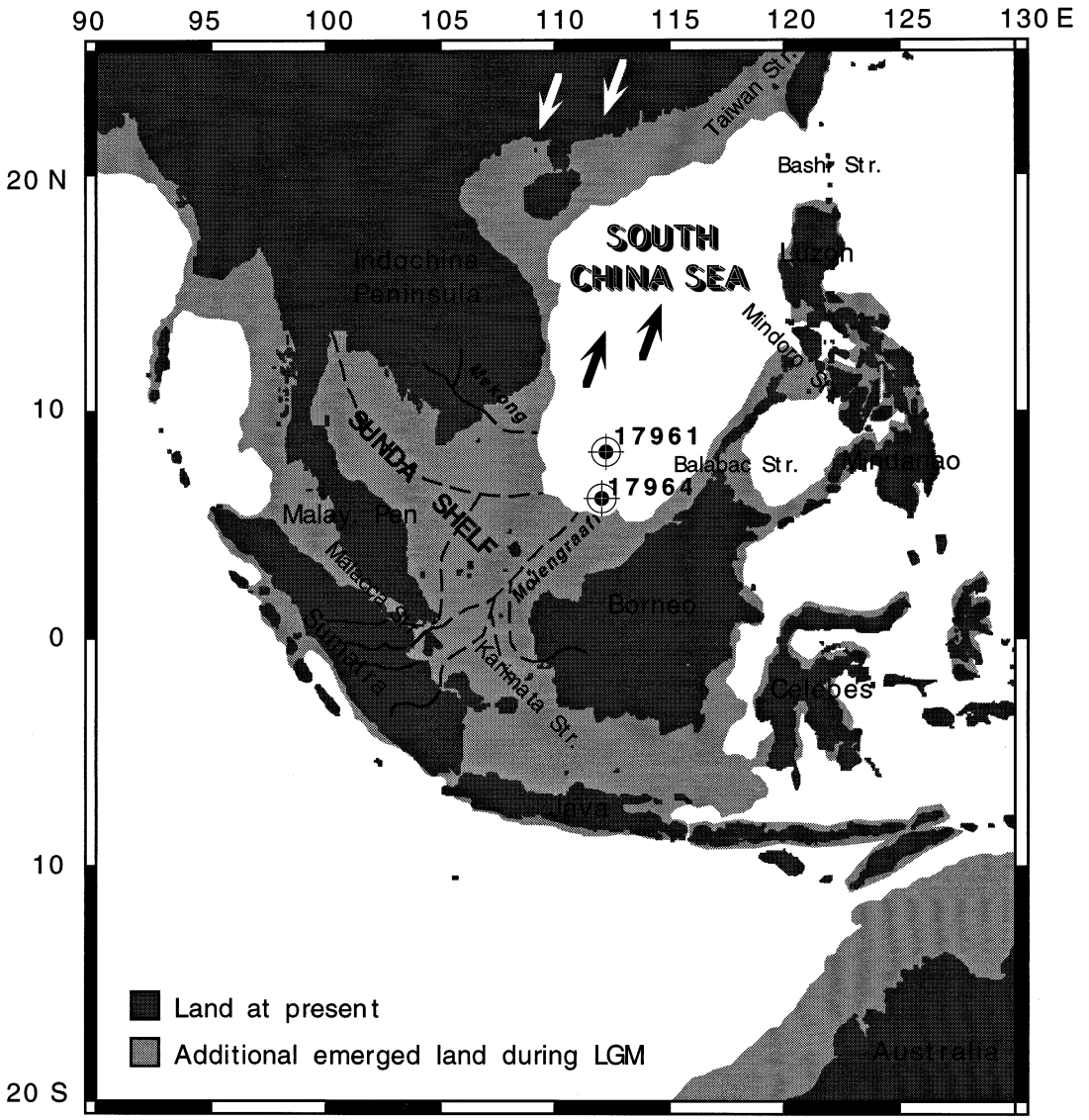

Fig. 1. Map of the South China Sea showing the location of gravity cores 17961 and 17964, collected during the R/V *Sonne* cruise in April–June 1994 [12]. The glacial drainage systems according to Molengraaff [6] and the additional emerged land during the LGM are also plotted. Thick arrows represent typical monsoonal wind directions during winter (white) and summer (black).

ability. Accordingly, the emergence and drowning of Sundaland, which today comprises roughly 5% of the areal extent of the WPWP, potentially had a significant impact on the monsoonal transport of moisture, and the hydrological and geochemical cycles of the western Pacific and, consequently, on global climate [9,10]. It is speculated that during glacial times a stable equatorial low pressure system developed over the Malay–Indonesian area, enhancing the Walker circulation and thereby establishing oceanic conditions similar to La Niña today [9,11]. Moreover, the opening and closing of the important oceanic gateways between the western subtropical Pacific and the tropical Indo-Pacific probably led to strong feedbacks in the modification of the hydrological conditions of the northwestern subtropical

Pacific during the Quaternary. Hence, knowledge about the timing and effects of the drowning of Sundaland is fundamental to the understanding of global climate change during deglaciation.

In order to study the timing and impact of the drowning of Sundaland, we analyzed two cores from the southern SCS covering the last 30,000 years. The present work is focused on isotopic, sedimentological and organic geochemical parameters.

2. Materials and methods

2.1. Sample material

Two cores, 17961-2 (8°30′N, 112°19′E) and 17964-3 (6°09′N, 112°12′E), were retrieved during the *Sonne* 95 cruise to the SCS at water depths of 1968 m and 1556 m, respectively (Fig. 1). Based on echo-sounding profiles, the recovered material consists of undisturbed hemipelagic sediments [12]. Core 17964-3 is located close to the shelf break, which was the glacial palaeo-coastline, while 17961-2 is situated about 300 km further off shore in the central southern SCS. These two cores are ideally located to monitor hydrographic changes off the shelf, and any off-shore gradients, including changes in material supply from the shelf, which are directly correlated with the emergence/drowning of Sundaland.

2.2. Age model

The age models of cores 17961 and 17964 (Fig. 2) are based on two and six accelerator mass spectrometry (AMS) ^{14}C dates, respectively, and on both benthic and planktonic foraminiferal oxygen isotope stratigraphy. Analog ages of 9.8 cal. ky BP have been assigned to the end of Termination 1b [13], 11.6 cal. ky BP to the end of the Younger Dryas [14], [15] and 17.2 cal. ky BP to the end of the Last Glacial Maximum (LGM) ([10]; per analogy to core 17940). The stratigraphic correlation of 17961 and 17964 is based on benthic (*Cibicidoides wuellerstorfi*) oxygen isotope data [10,16], with the heaviest values in both records defined as the end of the LGM (Fig. 2). In order to avoid artifacts due to the combination of the gravity (17964-3) and the piston core (17964-2) records, only the gravity core data are used at station 17964. This choice minimizes possible correlation errors between cores 17961 and 17964 [10].

2.3. Analytical techniques

Stable oxygen and carbon isotopes were measured on samples of 15–20 and 2–10 specimens of *Globigerinoides ruber* s.s. (white) and *Cibicidoides wuellerstorfi*, respectively, in the 315–400 μm size fraction [10,16], providing a record of the isotopic composition of the upper 30 m of the water column (*G. ruber*; [17,18]) and the bottom water (*C. wuellerstorfi*; [19]). All tests were manually crushed, repeatedly washed in ethanol (99.8%) in an ultrasonic bath, and dried at 40°C. Samples (7–12 mg) of *Globigerinoides sacculifer* (core 17961; [10]) and *G. ruber* (core 17964; [16,10]) were used for AMS-^{14}C dating. Stable isotope ratios and AMS-^{14}C ages were determined at the Leibniz Laboratory of Kiel University following standard procedures [20]. The external errors of stable isotope analyses are ±0.08‰ PDB and ±0.06‰ PDB for $\delta^{18}O$ and $\delta^{13}C$, respectively. The average zero background of AMS-^{14}C dating is 0.3% ^{14}C (equal to about 46 ky BP). In the following text, ages in ky BP will always refer to calendar ages, which were obtained using the CALIB 3.03 software [21] and Winn et al. [13].

Siliciclastic clay contents were measured on the inorganic (H_2O_2 insoluble), decarbonated (HCl insoluble) fraction <63 μm of the sediment, using a SediGraph 5100D [22]. Clay mineral coagulation was avoided by use of undried samples. Additionally, 5 ml of 0.05% sodium-polyphosphate were added [23] to 80 ml of sediment suspension (3–6 g) and dispersed in an ultrasonic bath (5 min; [24]) prior to the measurement. The accuracy of the method was tested by clay content determination of replicate samples from core 17964 using the Atterberg settling technique (30 cm hight, 54 mm diameter; [25]) which yielded constantly 5.5% less clay [16]. This constant offset ($r = 0.94$) might be due to incomplete separation of the different fractions with the Atterberg columns and/or adsorption effects [26] using the SediGraph [16]. For comparative purposes (e.g. [10]), only the SediGraph results will be used in this manuscript.

Two different molecular biomarker families

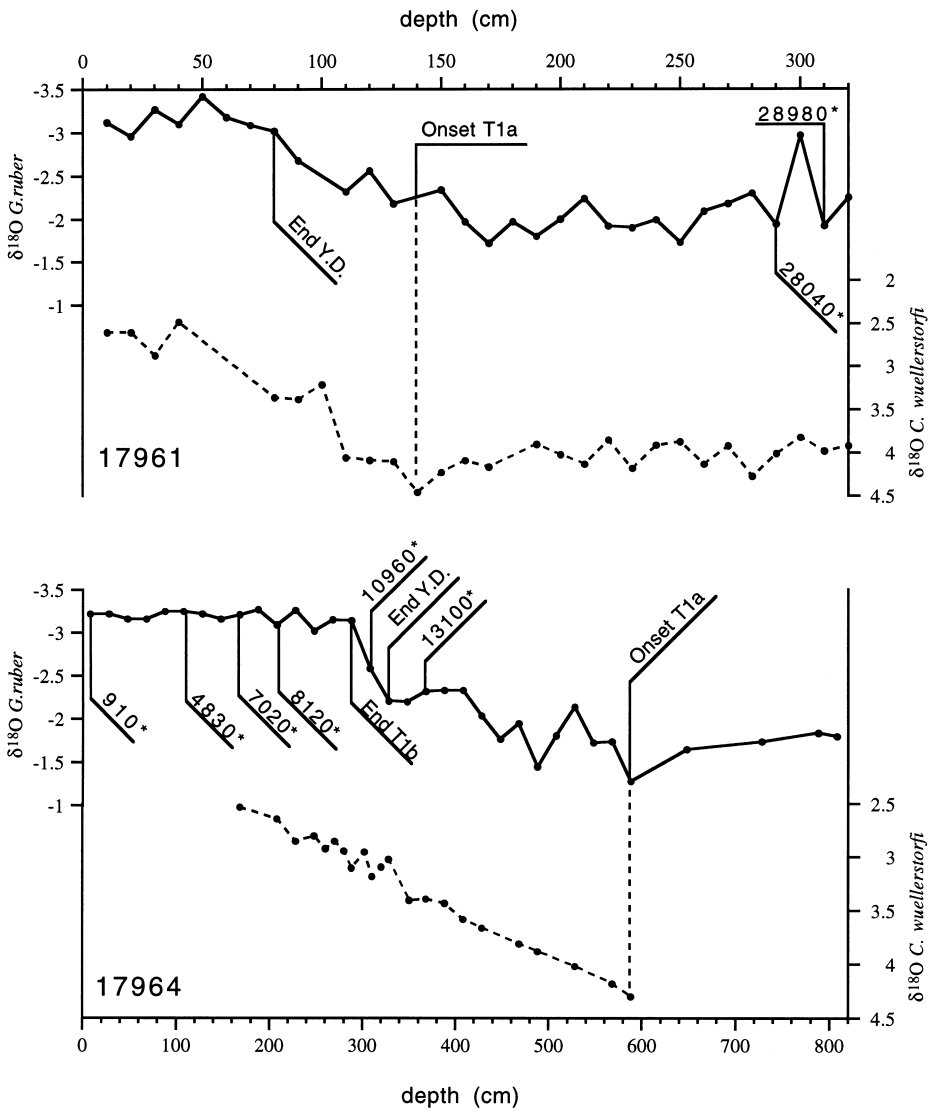

Fig. 2. Planktonic (*G. ruber*) and benthic (*C. wuellerstorfi*) foraminiferal $\delta^{18}O$ depth profiles of the cores studied in this work. The age control points in each core are indicated (see details in Wang et al. [10]). Values marked with an asterisk correspond to calibrated years (AMS-^{14}C ages are corrected by 400 years reservoir age according to Bard et al. [52] and converted to calendar years according to Stuiver and Braziunas [53], and Bard et al. [54]). Analog oxygen isotope chronostratigraphy ages of 9.8 cal. ky BP and 11.6 cal. ky BP were assigned to the end of Termination 1 (*End T1b* [13]) and the end of the Younger Dryas (*End Y.D.*; [14,15]), respectively. An age of 17.2 cal. ky BP was assigned to the end of the LGM (*Onset T1a* [10]), corresponding to the heaviest value in the benthic (*C. wuellerstorfi*) oxygen isotope record.

were studied: long chain alkanes and long chain alkenones. Long chain alkane distributions with predominance of odd-carbon-numbered members originate from higher plants [27]. For simplicity, only *n*-nonacosane was monitored as a marker of terrigenous organic matter since in all samples the alkane distributions had the characteristic odd to even carbon number predominance. C_{37} long chain alkenones were studied both as Haptophyte algae productivity tracers and for sea surface temperature (SST) as-

sessment using the U^K_{37} index [28]. The procedures and equipment for molecular biomarker determinations (*n*-nonacosane, C_{37} alkenones and the U^K_{37} index) are described elsewhere [29]. Briefly, sediment samples were freeze-dried and manually ground for homogeneity. After addition of an internal standard containing *n*-nonadecan-1-ol, *n*-hexatriacontane and *n*-tetracontane, dry subsamples (ca. 3 g) were extracted with dichloromethane in an ultrasonic bath. The extracts were hydrolyzed with 6% potassium hydroxide in methanol for the elimination of wax ester interferences. The *n*-hexane extracts were then evaporated under a N_2 stream, derivatized with bis(trimethylsilyl)trifluoroacetamide and analyzed by gas chromatography with flame ionization detection. Selected samples were examined by gas chromatography–mass spectrometry for confirmation of compound identification and evaluation of possible coelutions. Five replicates of a sediment sample with similar lipid content and U^K_{37} index showed a standard deviation of ± 0.15ºC in temperature estimation. The equation used for conversion of the U^K_{37} index into SST was $U^K_{37} = 0.031\mathrm{SST} + 0.092$, representing the annual mean temperature in the 0–30 m depth interval in the SCS [30,31].

Local sea surface salinities (SSS) were estimated from the variations in SST (U^K_{37}) and global ice-volume (*G. ruber*$_{\text{-white-}}$ δ^{18}O; [32]) using the transfer equation of Wang et al. [33].

3. Results and discussion

3.1. Description of core records 17961 and 17964

Major changes in sedimentation rates between the two cores and between glacial/interglacial periods in each core are evident from the age–depth relationships (Fig. 2). In core 17961, the sedimentation rate decreases from about 14 cm/ky during the glacial stage to 7 cm/ky during the Holocene. On the other hand, core 17964, which is located closer to the continental shelf, has significantly higher values, about 50 cm/ky during the glacial and 25 cm/ky during the interglacial.

During the last 30 ka, the most prominent changes in our records occurred at about 15–13.5 and 11.5–10 ky BP (Figs. 3 and 4) as a result of major changes in sea level (i.e. position of the coastline) and synchronous with changes in monsoon intensity, as reflected in palaeo-SST and palaeoproductivity records from the SCS [34,35]. The largest changes in both records are observed at 15–13.5 ky BP, corresponding to MWP Ia (termed as in ref. [36]). The SSTs in both cores show a synchronous, abrupt increase of 1.5ºC. This rise in SST is paralleled by a drop in clay and *n*-nonacosane contents to low Holocene levels, although low amplitude changes in absolute *n*-nonacosane concentrations in core 17961 make this event less clearly resolved at this site. However, after 14 ky BP, *n*-nonacosane abundances converge to the same values in both records, in contrast to the five-fold difference during the last glacial. Centered at about 14 ky BP, C_{37} alkenone concentrations in 17964 display a maximum which extends from about 16 to 11 ky BP, while the concentrations in 17961 decrease at 16 ky BP and remain at relatively low values compared to those in 17964.

The second major change in the records terminates at about 10 ky BP, 1000 year after MWP Ib (termed as in ref. [36]). Both δ^{18}O curves show a final decrease of about 0.7–1.0‰ and remain at Holocene levels thereafter (Fig. 3). SST estimates reach the Holocene level of about 28ºC at $\sim$7 ky BP, after a continuous rise since 15 ky BP. Thus, the overall SST increase associated with Termination I is about 2.6–2.8ºC which, as has been discussed elsewhere [31], is larger than the U^K_{37}-SST differences observed at open ocean sites from the same latitudes [37–39]. Estimates of SSS at both sites display a remarkable convergence to the same Holocene values, in contrast to the divergent trend during the deglaciation (Fig. 4). *G. ruber* δ^{13}C values for both locations start to increase simultaneously, however, reaching Holocene values only at about 7 ky BP.

3.2. Major factors controlling the palaeoceanography of the southern SCS on glacial–interglacial timescales

Today, tropical Indo-Pacific waters are advected into the SCS through the Malacca and Karimata straits [40,41]. Due to the low sill depths of these two channels (ca. 30 m; [3]), the connection of the SCS to the tropical Indo-Pacific was blocked during sea level stands below 30 m [42] (Fig. 1).

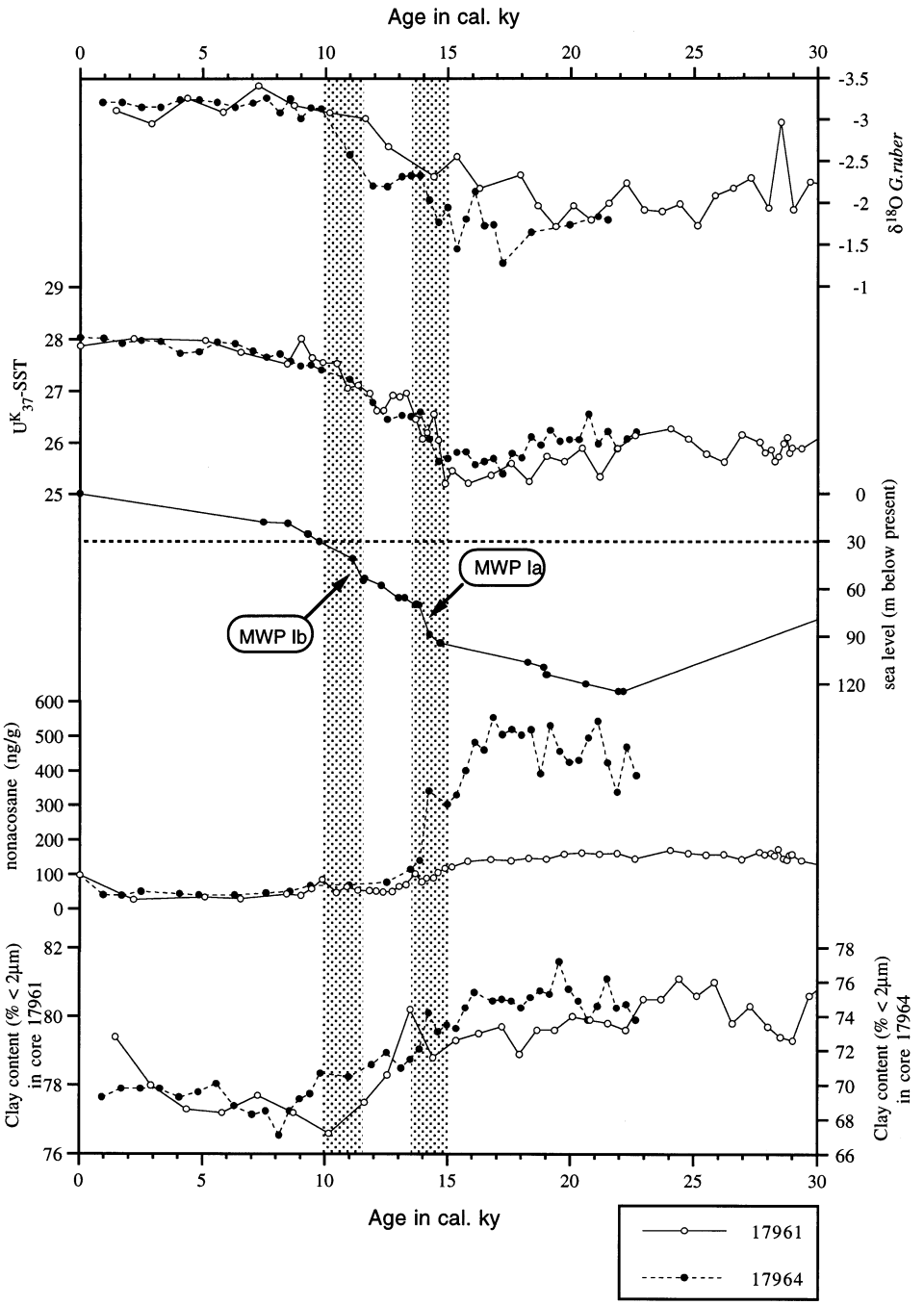

Fig. 3. Results of several key parameters studied in this work directly affected by the flooding of Sundaland: *G. ruber* $\delta^{18}O$, annual mean U^{K}_{37}-SST (0–30 m depth), *n*-nonacosane concentration and clay content. The sea level data used for discussion are from Fairbanks [32] and Bard et al. [52]. Shaded vertical bars correspond to time intervals of major changes in the southern SCS as discussed in the text. *MWP Ia* and *Ib* are labeled according to [36]. The horizontal dashed line corresponds to the time when sea level reached 30 m below present.

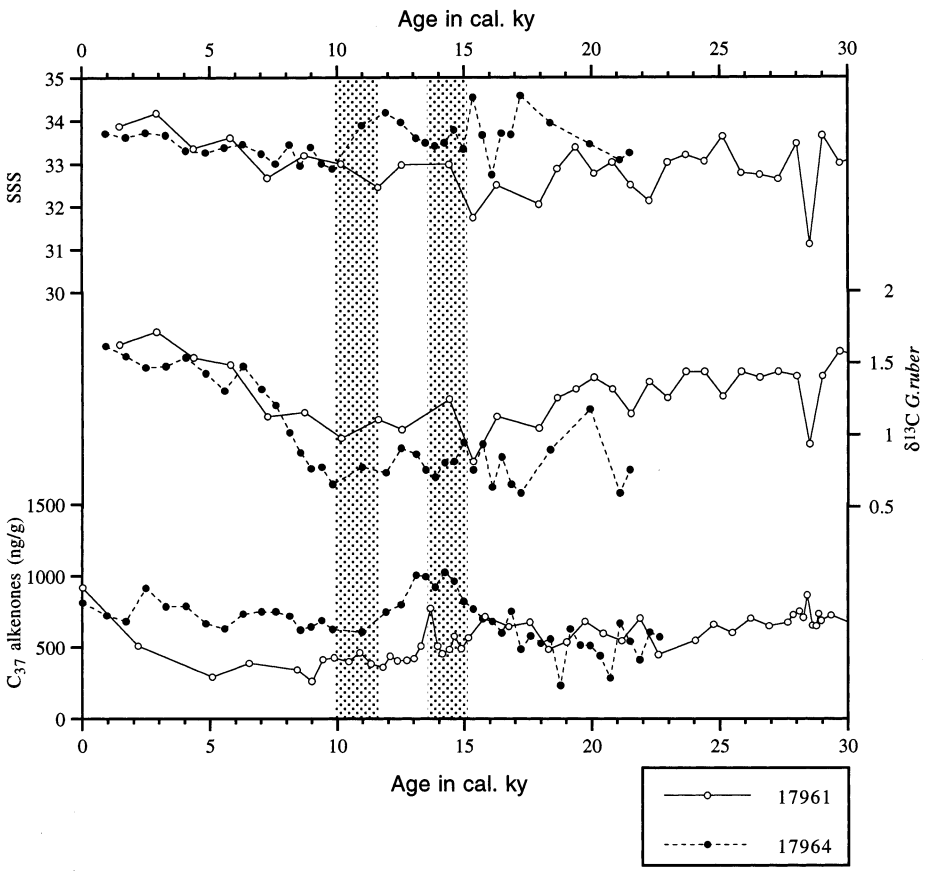

Fig. 4. Results of other parameters studied in this work likely to have been affected by the flooding of the Sunda Shelf: sea surface salinity (SSS), *G. ruber* $\delta^{13}C$ and C_{37} alkenone concentration. Shaded vertical bars correspond to time intervals of major changes in the southern SCS as discussed in the text. MWP Ia and Ib are labeled according to [36].

The Sunda Shelf is the largest shelf area in the world, with average water depths of 70 to 80 m [1,2]. During its emergence at the LGM this lowland was drained by major streams [6]. One of them, the so-called Molengraaff River, debouched close to site 17964 (Fig. 1).

Previous studies of Asian palaeomonsoon variability have concluded that the winter monsoon was stronger during glacial periods [10,34,35], which brought moisture from the tropical–subtropical western Pacific to the emergent Sundaland. Although the summer monsoon weakened in glacial and strengthened in interglacial periods [10,34,35], it also contributed to the precipitation over Sundaland by transporting water vapour from the eastern Indian Ocean area.

The deglacial rise in sea level is expected to have had critical impact on the interaction of these three variables and therefore on the SCS palaeoceanography.

3.3. The submergence of Sundaland

During the LGM, the Sunda Shelf was completely emergent. The extremely high content of *n*-nonacosane in the two core records (Fig. 3) at >15 ky BP with a five-fold offshore gradient of this terrigenous marker between 17964 and 17961 is due to the close proximity of site 17964 to the Molengraaff River mouth. This is also reflected by the higher proportion of clay-sized material in the glacial sections. SST was low, partly because no warm tropical wa-

ters entered the SCS due to the closure of the straits in the south. SSS estimates of core 17961 show slightly decreased levels compared to the Holocene (Fig. 4), possibly a result of the riverine freshwater influence, although salinity estimates should be considered with caution as will be discussed below.

At the beginning of the deglaciation the position of the river mouth remained unchanged during the first small step in sea level rise, due to the morphology of the shelf break. This is recorded by the continuously high clay and *n*-nonacosane concentrations at site 17964. However, the decreasing *G. ruber* $\delta^{13}C$ values at both sites could be interpreted as an increase in nutrient concentrations and marine productivity, which is also shown by the gradual rise in C_{37} alkenone concentration (Fig. 4). This may have resulted from coastal upwelling in front of the Sunda Shelf during summer [43] caused by the SW summer monsoonal wind which started to increase right after the summer insolation minimum at 22–20 ky BP [10].

The SSS estimates at 20 ky BP diverge significantly between 17964 and 17961 (Fig. 4), and, moreover, the salinity at the southernmost site increases while that at the northernmost decreases. This feature is counterintuitive, since 17964 is located closer to the Molengraaff River mouth and should thus display lower salinities. Two recent studies [44,45] have critically reviewed the basic assumptions involved in palaeo-SSS reconstructions by means of planktonic foraminiferal $\delta^{18}O$, ice-volume and SST data. In particular, one of the main assumptions is the constancy of the salinity vs. water $\delta^{18}O$ ratio with time, which is not obvious on glacial–interglacial timescales. Of relevance here, changes in the local freshwater budget could significantly affect the oxygen isotopic composition of sea water in marginal seas like the SCS [44,46,47] and thus render SSS reconstructions invalid. However, the higher SSS at station 17964 could also be a result of local upwelling as discussed previously.

Despite possible bias to the SSS reconstructions, our records clearly show that during the last 10 ka, the SSS reconstructions of both stations match very well. This convergence suggests the establishment of similar oceanographic conditions at both stations at that time, which is probably indicative of the complete flooding of Sundaland.

It is not until the sea level rise associated with MWP Ia at 15–13.5 ky BP that a fundamental change occurred in the oceanographic setting of the southern SCS. This change is clearly seen in the simultaneous SST rise at both stations and in the abrupt decrease of *n*-nonacosane concentrations (Fig. 3). The SST rise is in phase with the global warming at the beginning of the Bølling/Allerød. This temperature change might have been enhanced by the development of a vast shallow warm water pool over Sundaland, which was flooded by sea level rise across the threshold depth of −70 m. Additionally, a decrease in winter monsoon intensity [10] could have resulted in less advection of cool subtropical waters from the north through the Bashi Strait, further amplifying the SST signal. The rapid landward displacement of the river mouth (>200 m/year) probably created a vast trap for terrigenous material on the shelf, which led to an abrupt decrease in *n*-nonacosane abundances and lower sedimentation rates at both sites, as well as the diminishment of the glacial high gradient in *n*-nonacosane concentration between these two sites. This is also reflected in the decrease in clay content at site 17964 between 16 and 15 ky BP.

The last stage of the flooding and submergence of Sundaland was accomplished at about 10 ky BP, 1 ky after MWP Ib, leading to the establishment of the modern surface water connection with the tropical Indo-Pacific through the southern gateways (Fig. 1). This last period is characterized by the convergence of the $\delta^{18}O$ records in both cores, indicating the disappearance of tropical riverine influence and a strong homogenization of hydrographic properties. According to the sea level curve [32], the 30 m depth of the present Karimata Strait depth was reached at about 10 ky BP, in agreement with the convergence of our records (Fig. 3). In addition, the significantly intensified summer monsoon [10,35], which brings tropical warm waters into the SCS, resulted in the final rise of SST to the Holocene level. At both sites, the $\delta^{13}C$ of *G. ruber* reached its last minimum at 10 ky BP, followed by a monotonous increase to similar Holocene values at both sites at 7 ky BP. Similar deglacial $\delta^{13}C$ minima have been reported from other low latitude sites and these have been attributed to changes in the intensity of upwelling of intermediate waters [48], [49].

4. Conclusions

Two distinct periods of sedimentological, foraminiferal isotopic and organic geochemical changes are recognized in two cores from the southern SCS, associated with different levels of flooding of the Sundaland.

The main changes occurred at about 15–13.5 ky BP, synchronously with MWP Ia. This initial flooding of Sundaland led to a strong decrease of terrigenous sediment supply at both the coastal and the off-shore core sites and was coincident with an abrupt 1.5ºC SST increase at both sites. Between 11.5 and 10 ky BP, the geochemical records of the coastal and off-shore core further rapidly converge, implying the establishment of similar oceanographic conditions at both sites roughly 1 ky after MWP Ib, and after the final opening of the gateways between the SCS and the tropical Indian Ocean.

Within dating uncertainties, the two steps of flooding of Sundaland seem to coincide with reorganizations in Asian monsoon climate as reconstructed from deep sea and lake sediment [35,10] and loess records [50,51]. Future climate modelling studies will have to evaluate possible feedbacks and/or amplification mechanisms between monsoonal climate, the land–sea configuration and the opening/closure of crucial gateways in the South-East Asian region.

Acknowledgements

The manuscript significantly benefited by comments from S.E. Calvert and official reviews by R. Fairbanks and an anonymous reviewer. Thanks are also due to M. Sarnthein for valuable discussions and dedication to South China Sea studies. CP thanks a Ph.D. grant from C.I.R.I.T. (Generalitat de Catalunya). MK acknowledges funding from the German Academic Exchange Program (DAAD) and later from a University of British Columbia Graduate Fellowship during the preparation of the manuscript. LW thanks the Deutsche Forschungsgemeinschaft for support in the study. Financial support from the TEMPUS EU project (ENV4-CT97-0564) is acknowledged. The samples used in this study were collected during a R/V *Sonne* cruise, funded by the German Ministry for Education and Research (BMBF). ***[FA]***

References

[1] K. Stattegger, W. Kuhnt, H. Wong, C. Bühring, et al., Cruise report SONNE 115: Sundaflut — Sequence stratigraphy, late Pleistocene–Holocene sea level fluctuations and high resolution record of the post-Pleistocene transgression on the Sunda Shelf, Berichte – Reports, Geol. Paläontol. Inst. Univ. Kiel, 86 (1997) 211 pp.

[2] P. Wang, Response of Western Pacific marginal seas to glacial cycles: paleoceanographic and sedimentological features, Mar. Geol. 156 (1999) 5–39.

[3] W.H.F. Smith, D.T. Sandwell, Global sea floor topography from satellite altimetry and ship depth soundings, Science 277 (1997) 1956–1962.

[4] A. Gupta, A. Rahman, W. Poh Poh, J. Pitts, The old alluvium of Singapore and the extinct drainage system to the South China Sea, Earth Surface Process. Landforms 12 (1987) 259–275.

[5] J.H.F. Umbgrove, Structural History of the East Indies, Cambridge University Press, Cambridge, 1949.

[6] G.A.F. Molengraaff, Modern deep-sea research in the East Indian Archipelago, Geogr. J. 57 (1921) 95–121.

[7] P.J. Webster, The role of hydrological processes in ocean–atmosphere interactions, Rev. Geophys. 32 (1994) 427–476.

[8] K.E. Trenberth, G.W. Branstator, D. Karoly, A. Kumar, N.-C. Lau, C. Ropelewski, Progress during TOGA in understanding and modeling global teleconnections associated with tropical sea surface temperatures, J. Geophys. Res. 103 (1998) 14291–14324.

[9] W.H. Quinn, Late Quaternary meteorological and oceanographic developments in the equatorial Pacific, Nature 229 (1971) 330–331.

[10] L. Wang, M. Sarnthein, H. Erlenkeuser, J.O. Grimalt et al., East Asian monsoon climate during the late Pleistocene: high-resolution sediment records from the South China Sea, Mar. Geol. 156 (1999) 243–282.

[11] S.W. Hostetler, A.C. Mix, Reassessment of ice-age cooling of the tropical ocean and atmosphere, Nature 399 (1999) 673–676.

[12] M. Sarnthein, U. Pflaumann, P.X. Wang, H.K. Wong, Preliminary report of the *Sonne*-95 cruise 'Monitor Monsoon' to the South China Sea, Berichte – Reports, Geol. Paläontol. Inst. Univ. Kiel 68 (1994) 225 pp.

[13] K. Winn, M. Sarnthein, H. Erlenkeuser, $\delta^{18}O$ stratigraphy and chronology of Kiel sediment cores from the East Atlantic, Berichte – Reports, Geol. Paläontol. Inst. Univ. Kiel 45 (1991) 99 pp.

[14] P.M. Grootes, M. Stuiver, Oxygen 18/16 variability in Greenland snow and ice with 10^{-3} to 10^{5}-year time resolution, J. Geophys. Res. 102 (1997) 26455–26470.

[15] T. Goslar, M. Arnold, E. Bard, T. Kuc et al., High concentration of atmospheric ^{14}C during the Younger Dryas cold episode, Nature 377 (1995) 414–417.

[16] M. Kienast, Geschichte des Flusseintrags vom Sunda-Schelf: Abbild in hemipelagischen Sedimenten aus dem Südchinesischen Meer, Unpubl. Diplom-Thesis, Kiel University, 1996, 53 pp.
[17] R.G. Fairbanks, P.H. Wiebe, A.W.H. Bé, Vertical distribution and isotopic composition of living planktonic foraminifera in the Western North Atlantic, Science 207 (1980) 61–63.
[18] R.G. Fairbanks, M. Sverdlove, R. Free, P.H. Wiebe, A.W.H. Bé, Vertical distribution and isotopic fractionation of living planktonic foraminifera from the Panama Basin, Nature 298 (1982) 841–844.
[19] R. Zahn, K. Winn, M. Sarnthein, Benthic foraminiferal $\delta^{13}C$ and accumulation rates of organic carbon: *Uvigerina peregrina* group and *Cibicidoides wuellerstorfi*, Paleoceanography 1 (1986) 27–42.
[20] M. Schleicher, P.M. Grootes, M.J. Nadeau, A. Schoon, ^{14}C backgrounds and their components at the Leibniz AMS facility, Radiocarbon 40 (1998).
[21] M. Stuiver, P.J. Reimer, Extended ^{14}C data base and revised Calib 3.0 ^{14}C age calibrated program, Radiocarbon 35 (1993) 215–230.
[22] R. Stein, Rapid grain-size analysis of clay and silt fraction by SediGraph 5000D: comparison with Coulter Counter and Atterberg methods, J. Sediment. Petrol. 55 (1985) 590–615.
[23] D.M. Moore, R.C. Reynolds Jr., X-Ray Diffraction and the Identification and Analysis of Clay Minerals, 1989, 332 pp.
[24] J.P. Coakley, J.P.M. Syvitski, SediGraph technique, in: J.P. Syvitski (Ed.), Principles, Methods, and Applications of Particle Size Analysis, Cambridge University Press, Cambridge, 1991, pp. 129–142.
[25] G. Müller, Methoden der Sedimentuntersuchung Teil 1, Schweizerbart'sche Verlagsbuchhandlung, 1964.
[26] I.N. McCave, J.P.M. Syvitski, Principles and methods of geological particle size analysis, in: J.P.M. Syvitski (Ed.), Principles, Methods, and Applications of Particle Size Analysis, Cambridge University Press, Cambridge, 1991, pp. 3–21.
[27] G. Eglinton, R.J. Hamilton, Leaf epicuticular waxes, Science 156 (1967) 1322–1335.
[28] S.C. Brassell, G. Eglinton, I.T. Marlowe, U. Pflaumann, M. Sarnthein, Molecular stratigraphy: a new tool for climatic assessment, Nature 320 (1986) 129–133.
[29] J. Villanueva, C. Pelejero, J.O. Grimalt, Clean-up procedures for the unbiassed estimation of C_{37}–C_{39} alkenones sea surface temperatures and terrigenous *n*-alkane inputs in paleoceanography, J. Chromatogr. 757 (1997) 145–151.
[30] C. Pelejero, J.O. Grimalt, The correlation between the Uk37 index and sea surface temperatures in the warm boundary: the South China Sea, Geochim. Cosmochim. Acta 61 (1997) 4789–4797.
[31] C. Pelejero, J.O. Grimalt, S. Heilig, M. Kienast, L. Wang, High resolution U^{K}_{37}-temperature reconstructions in the South China Sea over the last 220 kyrs, Paleoceanography 14 (1999) 224–231.
[32] R.G. Fairbanks, The age and origin of the 'Younger Dryas climate event' in Greenland ice cores, Paleoceanography 5 (1990) 937–948.
[33] L. Wang, M. Sarnthein, J.C. Duplessy, H. Erlenkeuser, S. Jung, U. Pflaumann, Paleo sea surface salinities in the low-latitude Atlantic: the $\delta^{18}O$ record of *Globigerinoides ruber* (white), Paleoceanography 10 (1995) 749–761.
[34] L. Wang, P. Wang, Late Quaternary paleoceanography of the South China Sea: glacial–interglacial contrasts in an enclosed basin, Paleoceanography 5 (1990) 77–90.
[35] C.-Y. Huang, P.-M. Liew, M. Zhao, T.-C. Chang, C.-M. Kuo, M.-T. Chen, C.-H. Wang, L.-F. Zheng, Deep sea and lake records of the Southeast Asian paleomonsoons for the last 25 thousand years, Earth Planet. Sci. Lett. 146 (1997) 59–72.
[36] R.G. Fairbanks, A 17,000 year glacio-eustatic sea level record: influence of glacial melting rates on the Younger Dryas event and deep-ocean circulation, Nature 342 (1989) 637–642.
[37] F.G. Prahl, L.A. Muehlhausen, M. Lyle, An organic geochemical assessment of oceanographic conditions at MANOP Site C over the past 26,000 years, Paleoceanography 4 (1989) 495–510.
[38] E.L. Sikes, L. Keigwin, Equatorial Atlantic sea surface temperature for the last 30 ky: a comparison of U^{k}_{37}, $\delta^{18}O$ and foraminiferal assemblage temperature estimates, Paleoceanography 9 (1994) 31–45.
[39] N. Ohkouchi, K. Kawamura, T. Nakamura, A. Taira, Small changes in the sea surface temperature during the last 20,000 years: molecular evidence from the western tropical Pacific, Geophys. Res. Lett. 21 (1994) 2207–2210.
[40] K. Wyrtki, Scientific results of marine investigations of the South China Sea and the Gulf of Thailand. Physical Oceanography of the Southeast Asia Waters, in: NAGA Report 2, Scripps Institution of Oceanography, La Jolla, CA, 1961, 195 pp.
[41] Y. Masumoto, T. Yamagata, Simulated seasonal circulation in the Indonesian Sea, J. Geophys. Res. 98 (1993) 12501–12509.
[42] P. Wang, L. Wang, Y. Bian, Z. Jian, Late Quaternary paleoceanography of the South China Sea: surface circulation and carbonate cycles, Mar. Geol. 127 (1995) 145–165.
[43] S.-Y. Chao, P.-T. Shaw, S.Y. Wu, Deep water ventilation in the South China Sea, Deep Sea Res. 43 (1996) 445–466.
[44] E.J. Rohling, G.R. Bigg, Paleosalinity and $\delta^{18}O$: a critical assessment, J. Geophys. Res. 103 (1998) 1307–1318.
[45] G.A. Schmidt, Error analysis of paleosalinity calculations, Paleoceanography 14 (1999) 422–429.
[46] M.K. Gagan, L.K. Ayliffe, D. Hopley, J.A. Cali, G.E. Mortimer, J. Chappell, M.T. McCulloch, M.J. Head, Temperature and surface–ocean water balance of the Mid-Holocene tropical Western Pacific, Science 279 (1998) 1014–1018.
[47] J.C. Zachos, L.D. Stott, K.C. Lohmann, Evolution of early Cenozoic marine temperatures, Paleoceanography 9 (1994) 353–387.
[48] D.W. Oppo, R.G. Fairbanks, Carbon isotope composition of tropical surface water during the past 22,000 years, Paleoceanography 4 (1989) 333–351.

[49] B.K. Linsley, R.B. Dunbar, The late Pleistocene history of surface water $\delta^{13}C$ in the Sulu Sea: possible relationship to Pacific deepwater $\delta^{13}C$ changes, Paleoceanography 9 (1994) 317–340.
[50] Z. An, S.C. Porter, W. Zhou, Y. Lu, D.J. Donahue, M.J. Head, X. Wu, J. Ren, H. Zheng, Episode of strengthened summer monsoon climate of Younger Dryas age on the Loess Plateau of central China, Quat. Res. 39 (1993) 45–54.
[51] S.C. Porter, Z. An, Correlation between climate events in the North Atlantic and China during the last glaciation, Nature 375 (1995) 305–308.
[52] E. Bard, B. Hamelin, R.G. Fairbanks, A. Zindler, Calibration of the ^{14}C timescale over the past 30,000 years using mass spectrometric U–Th ages from Barbados corals, Nature 345 (1990) 405–410.
[53] M. Stuiver, T.F. Braziunas, Modeling atmospheric ^{14}C influences and ^{14}C ages of marine samples to 10,000 BC, Radiocarbon 35 (1993) 137–189.
[54] E. Bard, B. Hamelin, R.G. Fairbanks, U–Th ages obtained by mass spectrometry in corals from Barbados: sea level during the past 130 000 years, Nature 346 (1990) 456–458.